TIME-DISTANCE MEASUREMENTS OF SUBSURFACE ROTATION AND MERIDIONAL FLOW

P.M. Giles[1], T.L. Duvall, Jr.[2], P.H. Scherrer[3]

[1]Dept of Applied Physics, Stanford University, Stanford, CA 94305-4085 USA pgiles@solar.stanford.edu
[2]Laboratory for Astronomy and Solar Physics, NASA/Goddard Space Flight Center, Greenbelt, MD 20771 USA
[3]W.W Hansen Experimental Physics Laboratory, Stanford University, Stanford, CA 94305-4085 USA

ABSTRACT

Large-scale flows in the solar convection zone are interesting because of the part they might play in the eleven-year magnetic cycle (Wang et al. 1991; Dikpati & Choudhuri 1995; Gilman & Miller 1986). The emerging technique of time-distance helioseismology has proven to be a very useful tool for measuring such flows (Giles et al. 1997; Giles & Duvall 1998). Here we present work which extends the previous results, using data from the MDI instrument on SOHO.

Key words: time-distance helioseismology; meridional flow; rotation

1. INTRODUCTION

One of the most successful applications of time-distance helioseismology has been the search for flows in the solar convection zone. The technique can potentially allow us to map the flow pattern beneath the solar surface. Previous applications have included a search for local flows in and around sunspots (Duvall et al. 1996), and an examination of the near-surface rotation (Duvall et al. 1998).

More recently, the time-distance method has been applied to the measurement of flows on a larger scale. One flow of particular interest to theorists is the flow in meridian planes, known as the meridional circulation. Surface measurements made from direct Doppler observations (Duvall 1979; Labonte & Howard 1982; Hathaway et al. 1996) or tracking of magnetic features (Komm et al. 1997) have shown that this flow is poleward in both hemispheres, with the measured magnitudes ranging from 10 to 30 m/s. Our first efforts to measure the subsurface meridional flow using time-distance helioseismology revealed that the poleward flow extended to a depth of at least 26 Mm, with a depth-averaged magnitude of (23.5 ± 0.6) m/s at mid-latitude (Giles et al. 1997). Since that time, measurements using other techniques have confirmed some of these conclusions (Schou & Bogart 1998; González Hernández et al. 1998).

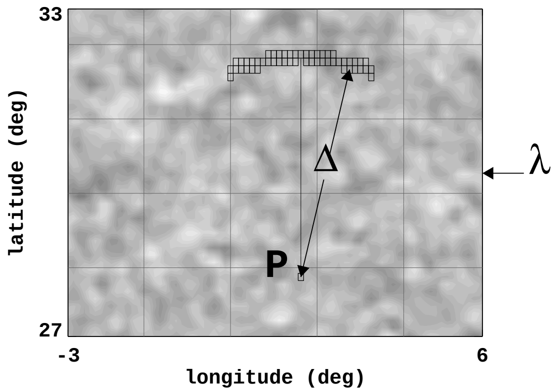

Figure 1. This schematic depiction of the method used for measuring the meridional flow shows a small portion of an MDI doppler image, remapped and then filtered to remove low-frequency noise. The velocity signal in pixel P is cross correlated with the signal in each of the pixels in the arc outlined above. The process is repeated for all the other pixels which have the same latitude as P. The resulting cross correlations are averaged together to determine the mean cross correlation for latitude λ and distance Δ. Note that when measuring the rotation the situation is changed so that the correlated pairs lie in an east-west orientation instead of a north-south one.

The time-distance method has also been applied to the measurement of the solar differential rotation. Although the rotation of the solar interior is already known very accurately from splittings of normal mode frequencies (Schou et al. 1998), that technique is only sensitive to the component of rotation which is symmetric in latitude. Surface Doppler measurements (Hathaway et al. 1996; Ulrich 1998) have shown that the rotation rate of the photosphere is not the same in the northern and southern hemispheres. By applying the time-distance method, Duvall et al. (1998) have shown that this asymmetry extends below the surface as well. We extended this observation to cover an entire solar rotation and concluded that during the summer of 1996 the solar southern hemisphere was rotating slightly more rapidly than the northern (Giles & Duvall 1998).

The following section outlines the method of applying time-distance helioseismology to large-scale flows. In the Results section, we show new results which extend our previous work to cover longer time periods and greater depths.

2. METHODS

Time-distance helioseismology relies on the measurement of acoustic wave travel times to infer details of the sun's interior structure (Duvall et al. 1997). The travel time between two points on the solar surface is measured by computing the temporal cross correlation of their velocity signals. The location of the peak in the cross correlation is then interpreted as the time required for a sound wave to propagate from one point to the other. In practice, it is necessary to average together cross correlations for many pairs of points. The travel time is determined by fitting a Gabor wavelet to the average cross correlation.

To measure flows, it is necessary to measure wave travel times in opposite directions along the same ray path. The time difference $\delta\tau$ between the two travel times is then related to the flow velocity $\mathbf{v}$ by

$$\delta\tau \simeq -2 \int_{\Gamma} \frac{\mathbf{v}\cdot\hat{\mathbf{n}}}{c^2} ds \qquad (1)$$

where $\hat{\mathbf{n}}ds$ is the length along the ray path Γ, and c is the sound speed.

By choosing different pairs of end points, one can select different ray paths, and hence probe the velocity in specific directions and at various locations. For example, to measure the meridional flow, it is necessary to choose pairs of points which lie along the same (or nearly the same) line of longitude (figure 1). In this case, the travel time difference is only sensitive to the north-south component of the flow, and

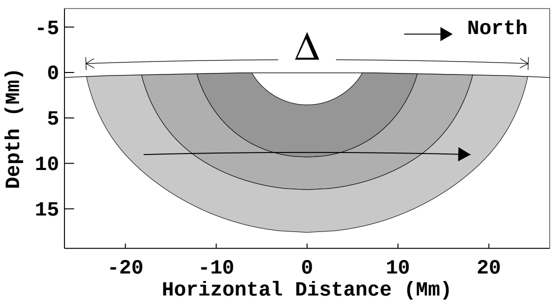

Figure 2. In the interpretation of time-distance measurements, acoustic waves are assumed to travel along narrow ray paths, which are determined by the sound speed profile below the surface. Waves which travel a larger distance Δ penetrate deeper into the interior. The solid curved arrow represents a hypothetical meridional flow through the region of ray propagation.

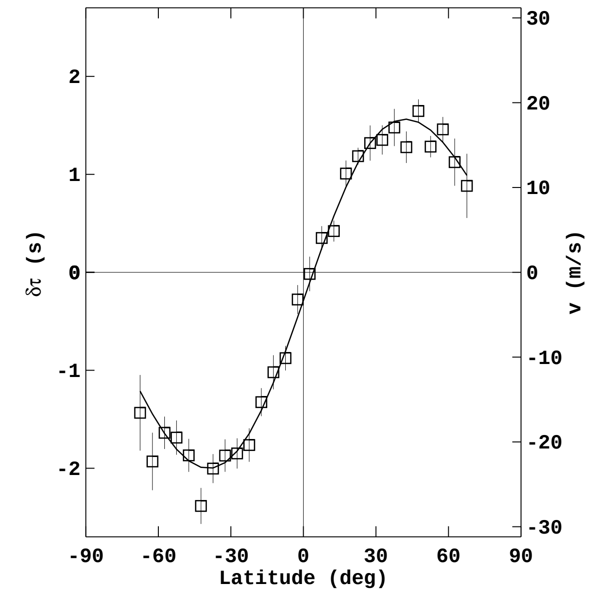

Figure 3. The squares represent the measured time differences $\delta\tau$ between southward and northward travel times, for a range of central latitudes λ. A positive time difference indicates a northward flow; hence the observations clearly show a poleward meridional flow in both hemispheres, with a small southward flow across the equator. The corresponding flow velocity (right-hand axis) was computed using equation (1) by assuming a uniform, horizontal flow throughout the region of propagation. The solid curve is a three-term least squares fit to the data (see text).

is not affected by the rotation.[1] Conversely, the rotation can be measured by choosing endpoints with the same (or nearly the same) latitude.

By varying the separation Δ between the endpoints, it is possible to probe different depths beneath the surface (figure 2). Thus, by measuring the travel times at different distances Δ and latitudes λ, we can determine the velocity $\mathbf{v}(r, \lambda)$ from equation (1).

For the results which follow, we have used Doppler images from the Michelson Doppler Imager (MDI) on SOHO. Almost all of the current work has been done with full-disk images from the summer of 1996 (May 24 – July 23). These images have a resolution of 2 arcseconds at disk center and a cadence of one minute. In spatial extent, the area studied extended to $\pm 80^\circ$ latitude and spanned 60° in longitude. This area was remapped onto a rectangular grid with pixels equally spaced in longitude and sine of latitude. The remapping was done for the entire two-month time series in eight-hour segments, and the cross correlations were computed (as described in figure 1) for each segment independently. In order to improve the signal-to-noise characteristics, the resulting cross correlations were averaged together in time before determining the travel times.

[1] note that although the endpoints in figure 1 do not all have the same longitude, the distribution of pixels is chosen to be symmetric with respect to the line of longitude that passes through P. The effect of rotation thus cancels out.

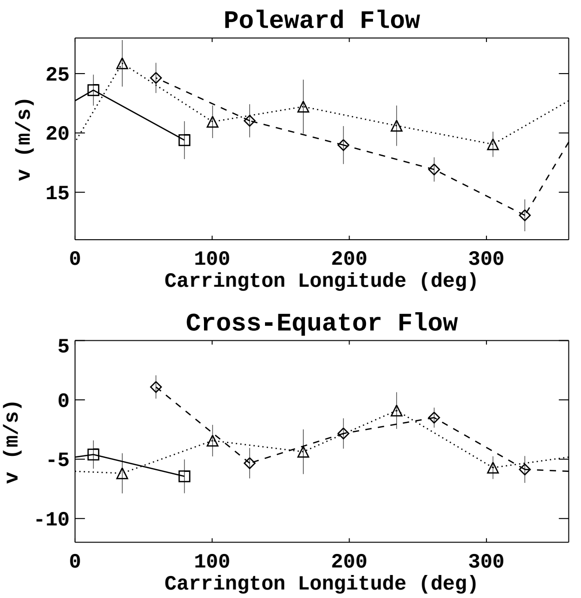

Figure 4. The two-month time series was divided into five-day segments in order to study the variability of the meridional flow. Shown in the upper figure is the amplitude of the poleward flow, and in the lower figure, the flow across the equator (negative values indicate southward velocities). In each plot, the three different symbols represent three different Carrington rotations (squares: 1909, triangles: 1910, and diamonds: 1911). Note that since each point represents five days of observations near the central meridian, it spans about sixty degrees in longitude.

The results presented in figure 6 and figure 10 also made use of the MDI medium-l program. The images in this observing mode are essentially full-disk Doppler images binned to 10 arcsecond spatial sampling. In this case there are far fewer cross correlations to compute; this makes it easier to push the observations to greater depths. The results shown here include 200 days of these observations from 1996. Because the computation of cross correlations is quite expensive in terms of computer resources, the extension of these measurements to even greater depths will have to rely on these lower-resolution images.

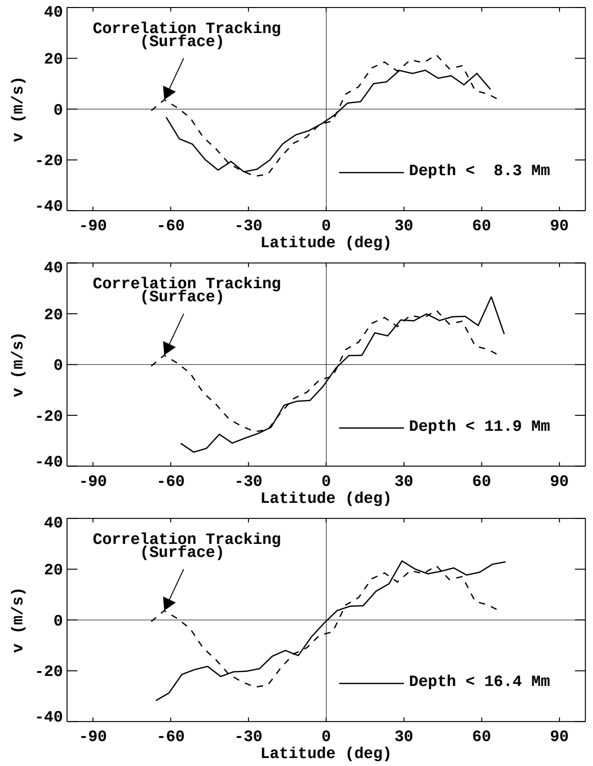

Figure 5. Depth variation of meridional flow. The three plots show time-distance measurements of the meridional flow (solid curves). The maximum penetration depth of the rays included increases from 8.3 Mm in the top plot, to 16.4 Mm in the bottom plot. With each measurement we have included the "surface" rate as measured by tracking features in MDI magnetograms (dashed curve). The magnetic meaurement was made during the same time period. The velocities for the time-distance measurements were calculated using the same assumptions as described for figure 3.

3. RESULTS

3.1. Meridional Flow

Figure 3 shows the meridional flow measured over the entire two-month observing run. In this case the measurement includes pairs of endpoints with separations as small as 1° and as large as 8°. This means that the maximum depth of penetration is 33.6 Mm below the surface; the velocity shown on the right-hand axis is an average over this subsurface region. This result is an improvement of the result published previously (Giles et al. 1997) in that it includes another month of observation and some additional improvements in the treatment of the data. A close examination shows that the most significant change has occurred at high latitudes, which is probably due to the low signal-to-noise ratio in the acoustic oscillations near the limb.

The solid curve in figure 3 is a three-term[2] fit to the measurements of the form

$$v(\lambda) = a_1 \sin\lambda + a_2 \sin 2\lambda + a_4 \sin 4\lambda \qquad (2)$$

with $a_1 = (-3.3 \pm 0.4)\,\mathrm{m/s}$, $a_2 = (20.3 \pm 0.5)\,\mathrm{m/s}$, and $a_4 = (-1.6 \pm 0.5)\,\mathrm{m/s}$.

Because figure 3 includes two months of data, it represents a measurement of the axisymmetric component of the meridional flow during the summer of 1996. By dividing the two-month time series into smaller segments, we can search for structure in the

[2]The inclusion of the a_1 term in equation (2) requires some explanation. The observed flow across the equator could be due to the solar rotation, since the direction of the rotation axis in the MDI images cannot be known exactly. If there was a small error in this angle, the solid-body component of the rotation would give rise to a meridional circulation with a $\sin\lambda$ dependence. In order to produce a southward flow of 3.3 m/s at the equator, the orientation of the MDI images would have to be about 5 arcminutes different from the nominal value.

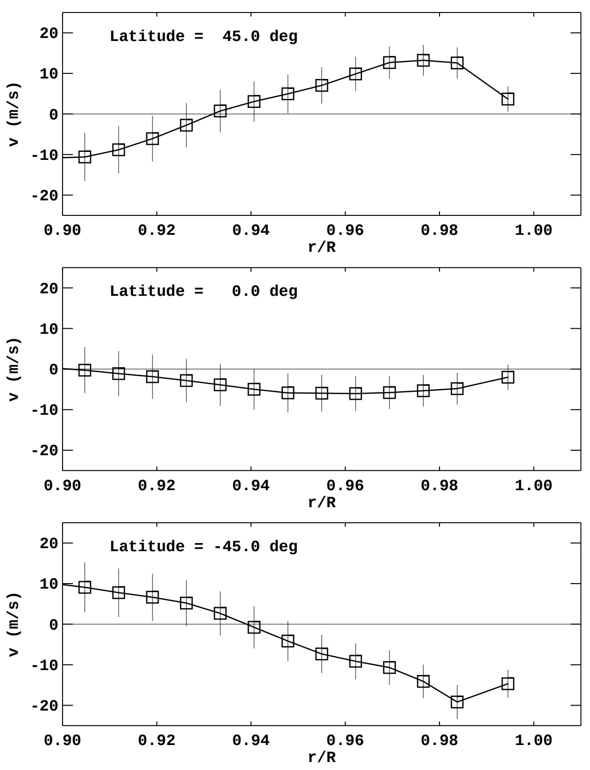

Figure 6. Inversion of meridional flow measurements. The three plots show the northward flow as a function of fractional radius. The upper plot is for 45° north latitude, the center plot is for the equator, and the lower plot for 45° south latitude.

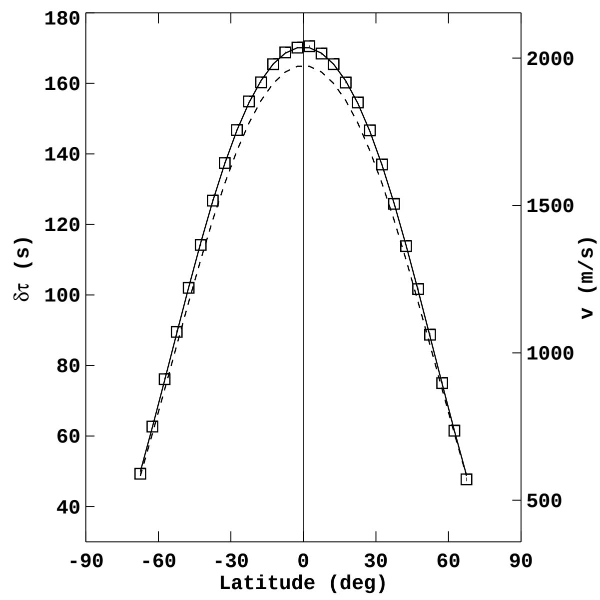

Figure 7. The squares represent the difference $\delta\tau$ between retrograde and prograde travel times, for a range of central latitudes λ. The velocity scale on the right-hand axis was computed using equation (1) by assuming a uniform, horizontal flow throughout the region of propagation. The dashed curve is a rotation rate derived from surface Doppler measurements by Ulrich et al. (1988). The solid curve is a four-term least squares fit to the data (see text).

flow pattern. Figure 4 shows two interesting aspects of the flow and how they vary with longitude. The upper plot shows the magnitude of the poleward flow (correspoding to a_2 in equation 2), while the lower plot shows the flow across the equator (corresponding to a_1). There are some hints of recurring structure, but it will require a longer time series before strong conclusions can be made. In the future, it might be particularly interesting to look for effects of magnetic activity on the local flow pattern.

It is also interesting to divide the data shown in figure 3 according to travel distance. In figure 5 we have made a simple attempt to examine the depth dependence of the flow by doing just this. Note that in the top plot, the rays included in the time-distance measurement have a maximum penetration depth of 8.3 Mm. Here, the subsurface flow matches the "surface" measurement quite well. In contrast, the bottom plot includes rays which penetrate further into the interior; the behaviour is quite different at high latitudes. This suggests that there is significant depth variation in the flow at high latitudes. Future work will examine this possibility more closely.

It should also be emphasized that the surface measurement shown in figure 5 was made during the same time period as the time-distance measurement. A previous study by Komm et al. (1997) using magnetic elements as tracers found that the peak meridional flow, averaged over a solar cycle, was only 13.2 m/s. However, the authors also found that the velocity was larger than average during solar minimum. If there is indeed a solar-cycle dependence in the meridional circulation, we should see the velocity decrease as the sun becomes more active. Future work will investigate this further.

Ultimately, the goal of this research is to go beyond the simple comparative approach shown in figure 5, and determine the entire velocity profile $\mathbf{v}(r, \lambda)$ from the measurements $\delta\tau(\Delta, \lambda)$. As a first attempt at this, we have used a two-dimensional regularized least-squares technique, with first-derivative regularization, to find the profile which best fits the data according to equation (1). The velocity is plotted versus the fractional radius for three different latitudes in figure 6. The inversion shows that the poleward flow seen near the surface becomes an equatorward flow below about 0.94 R, which corresponds to a depth of about 42 Mm. The southward flow at the equator is most prominent near the surface, and apparently disappears at greater depths.

Further study will be needed to better understand the limitations of the inversion procedure. The uncertainties and the spatial resolution will be of particular interest. In the following section we present a comparison of the time-distance inversion and the known interior rotation rate, which offers some measure of the reliability of this method.

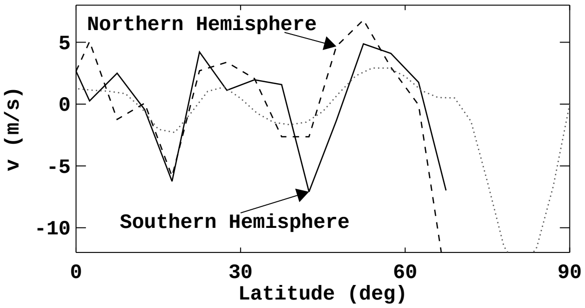

Figure 8. The smooth curve described by equation (3) has been subtracted from the time-distance measurements of the rotation (the squares in figure 7) to show the variation in the rotation rate on small scales. The solid and dashed curves represent the southern and northern hemispheres, respectively. For comparison, the dotted line is the measurement made by Kosovichev & Schou (1997) using f-mode frequency splittings.

3.2. Rotation

The measurement of the solar rotation proceeds exactly as that for the meridional flow, except that the ray endpoints are chosen to have the same (or nearly the same) latitude. Figure 7 shows the rotation rate measured over the entire two-month observing run. In this case the measurement includes end points with separations as small as 1° and as large as 10°. This means that the maximum depth of penetration is 41.9 Mm below the surface; the velocity shown on the right-hand axis is an average over this subsurface region. This result is an improvement of the result published previously (Giles & Duvall 1998) in that it includes another month of observation and some additional improvements in the treatment of the data. As with the meridional circulation, the most significant change has occurred at high latitude.

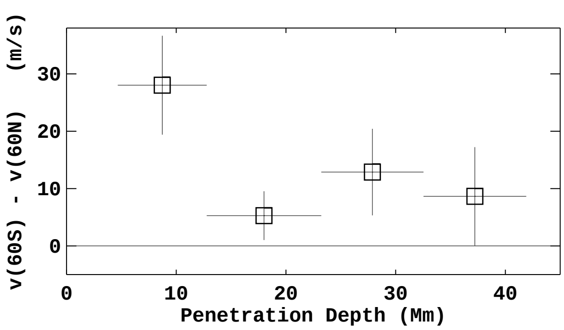

Figure 9. The quantity on the vertical axis is $v(\lambda = -60°) - v(\lambda = 60°)$, which is used as a simple measure of the rotational asymmetry. The velocity measurements have been made for four different ranges of travel distance; the horizontal error bars show the depth of penetration for each range.

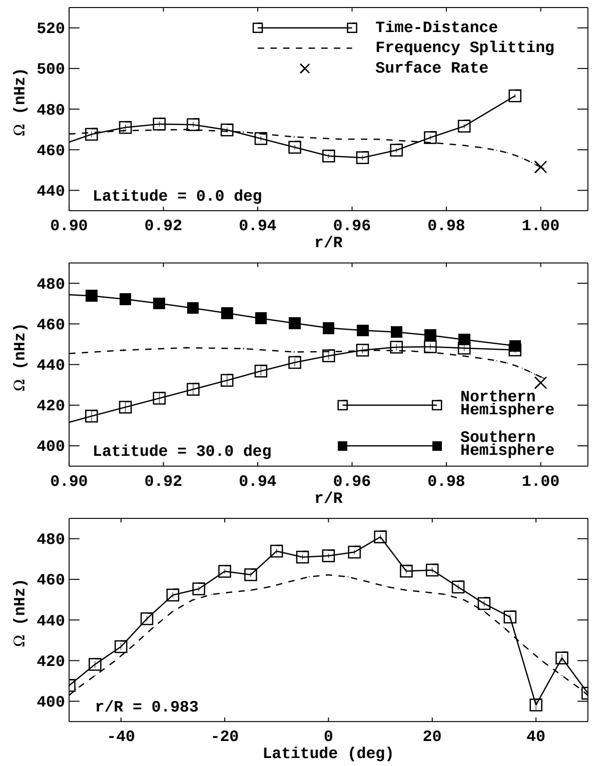

Figure 10. Inversion of rotation measurements. The three plots show the rotation rate (in nanohertz) derived from the time-distance measurements. The top figure shows the equatorial rate as a function of fractional radius, and the middle plot shows the rate at ±30° latitude. The bottom plot shows the variation with latitude at a depth of about 12 Mm. In each plot, the dashed curve was obtained by inversion of the MDI frequency splittings (Schou et al. 1998), and the points marked with an × from surface Doppler measurements (Ulrich et al. 1988).

The solid curve in figure 3 is a four-term fit to the measurements of the form

$$v(\lambda) = \cos\lambda \sum_{i=0}^{4} b_i \sin^i \lambda \qquad (3)$$

with $b_0 = (1997 \pm 1)\,\mathrm{m/s}$, $b_2 = (-187 \pm 12)\,\mathrm{m/s}$, $b_3 = (-19 \pm 5)\,\mathrm{m/s}$, and $b_4 = (-463 \pm 19)\,\mathrm{m/s}$. Note that the term in b_3 is antisymmetric about the equator[3].

In addition to the smooth rotation profile described by equation (3), there are significant variations on smaller scales. Bands of faster-than-average and slower-than-average rotation seem to be associated with latitudes of magnetic activity. These so-called "zonal flows" have been observed in the surface Doppler measurements (Howard & LaBonte 1980; Hathaway et al. 1996; Ulrich 1998) and, more recently, from splittings of f-mode frequencies (Kosovichev & Schou 1997). Figure 8 shows the results obtained using the time-distance method. The regions of fast rotation are clearly visible. If the flows do play an important part in the solar cycle, it will

[3] the value of the coefficient b_1 was not found to be significant and has been set to zero.

be interesting to study their depth dependence over longer time scales.

Another interesting feature of the rotation is the difference between the northern and southern hemispheres. Although it is not readily apparent in figure 7, the rotation measurements indicate that during the summer of 1996 the southern hemisphere was rotating more rapidly than the northern. In order to study the depth dependence of this effect, the time difference measurements were divided into four parts according to the travel distance. The westward velocity was computed for each set of measurements. As a simple measure of the asymmetry, figure 9 shows the difference in the rotational velocities measured at $\pm 60°$ latitude, where that difference is largest. The results suggest that the asymmetric rotation is most pronounced near the surface.

As with the meridional flow measurements, these simple methods of analyzing the depth dependence of the flows can often be quite illuminating. Ultimately, however, the goal is to recover the velocity profile of the entire convection zone. This requires a more sophisticated procedure, such as the least-squares inversion described in section 3.1.. In figure 10 we have applied that inversion to the rotation measurements and plotted the results for selected locations in the solar interior. As previously mentioned, the internal rotation of the sun is already very well known from analysis of normal mode frequency splittings. An inversion of these splittings is also shown in figure 10. This knowledge places a strong constraint on the time-distance measurements which should help in refining and improving the inversion techniques; the direct comparison is included to give a rough idea of the reliability of the time-distance method in its current state.

4. CONCLUSIONS

It is clear that time-distance helioseismology has the potential to reveal some details of large-scale flows which are inaccessible to modal techniques. Surface measurements made over the past decades have shown that these flows show significant variation with time. With the continued excellent performance of the MDI instrument and the SOHO spacecraft, we hope to extend this work through the rise to solar maximum and beyond.

It will also be interesting to push the measurements to deeper depths. For this, much more work needs to be done on the techniques and limitations of the inversion procedure, especially regarding the uncertainties and the spatial resolution of the results.

ACKNOWLEDGMENTS

This research is supported by NASA contract NAG5-3077 at Stanford University. The authors are indebted to Dr. Rick Bogart for providing and maintaining the remapping code.

REFERENCES

Dikpati, M., Choudhuri, A.R., 1995, Solar Physics 161, 9

Duvall, T.L. Jr., 1979, Solar Physics 63, 3

Duvall, T.L. Jr., D'Silva, S., Jeffries, S.M., Harvey, J.W., Schou, J., 1996, Nature 379, 235

Duvall, T.L. Jr., Kosovichev, A.G., Scherrer, P.H., et al., 1997, Solar Physics 170, 63

Duvall, T.L. Jr., Kosovichev, A.G., Scherrer, P.H., 1998. In: J. Provost, F.-X. Schmider (eds.) Proc. IAU Symp. 181, Sounding Solar and Stellar Interiors: Poster Volume. Observatoire de la Côte d'Azur, Nice, p. 169

Giles, P.M., Duvall, T.L. Jr., Scherrer, P.H., Bogart, R.S., 1997, Nature 390, 52

Giles, P.M., Duvall, T.L. Jr. 1998. In: Deubner, F.L. et al. (eds.) Proc. IAU Symp. 185, New Eyes to See Inside the Sun and Stars, Kluwer, Dordrecht, p.149

Gilman, P., Miller, J., 1986, ApJ 61, 585

González Hernández, I., Patrón, J., Bogart, R.S., et al., 1998, these proceedings

Hathaway, D.H., Gilman, P.A., Harvey, J.W., et al., 1996, Science 272, 1306

Howard, R., LaBonte, B., 1980, ApJ 239, L33

Komm, R.W., Howard, R.F., Harvey, J.W., 1993, Solar Physics 147, 207

Kosovichev, A.G., Schou, J. 1997, ApJ 482, L207

Labonte, B.J., Howard, R.F., 1982, Solar Physics 80, 361

Schou, J., Antia, H.M., Basu, S., et al., 1998, ApJ 505 (in press)

Schou, J., Bogart, R.S., 1998, ApJ Letters (in press)

Ulrich, R.K., Boyden, J.E., Webster, L., et al., 1988, Solar Physics 117, 291

Ulrich, R.K., 1998. In: Deubner, F.L. et al. (eds.) Proc. IAU Symp. 185, New Eyes to See Inside the Sun and Stars, Kluwer, Dordrecht, p. 59

Wang, Y.-M., Sheeley, N.R. Jr., Nash, A.G., 1991, ApJ 383, 431